

LETTER

Optimization of barrier height in InGaN quantum wells for rapid interwell carrier transport and low nonradiative recombination

To cite this article: Rinat Yapparov et al 2020 Appl. Phys. Express 13 122005

View the <u>article online</u> for updates and enhancements.

LETTER

Optimization of barrier height in InGaN quantum wells for rapid interwell carrier transport and low nonradiative recombination



Rinat Yapparov^{1*}, Cheyenne Lynsky², Shuji Nakamura², James S. Speck², and Saulius Marcinkevičius¹

Received October 29, 2020; accepted November 5, 2020; published online November 20, 2020

Rapid interwell carrier transport is a key process for a uniform carrier distribution and reduced Auger recombination in multiple quantum well (MQW) light emitting devices. In this work, the interwell transport has been studied by time-resolved photoluminescence in $In_{0.12}Ga_{0.88}N$ MQWs with $In_xGa_{1-x}N$ ($x=0 \div 0.06$) and $Al_{0.065}Ga_{0.935}N$ barriers. Only for the InGaN barriers the transport is efficient. However, introduction of In into the barriers is accompanied by an increase of the nonradiative recombination at QW interfaces. Still, even with the increased Shockley–Read–Hall recombination, structures with InGaN barriers might be advantageous for high power devices because of the reduced Auger recombination. © 2020 The Japan Society of Applied Physics

or an efficient operation of high power GaN/InGaN multiple quantum well (MQW) light emitting diodes (LEDs) and laser diodes, a uniform carrier distribution between the QWs is required. In such a case, all QWs contribute to the light emission, and a high output power can be achieved at relatively low carrier concentrations, at which the detrimental nonradiative Auger recombination can be kept at minimum. The limiting process for the uniform interwell (IW) carrier distribution is the transport of holes.

1-6) At room temperature, this transport is thermionic and proceeds via subsequent capture into and thermionic emission out of the QWs. Even in low In content (12%) InGaN/GaN QWs, the thermionic IW hole transport is slow and inefficient. An increase of the IW transport velocity can be achieved by replacing GaN barriers with that of InGaN.

However, the uniform IW carrier distribution and reduced Auger recombination are not the only factors affecting the efficiency of high power light emitting devices. The internal quantum efficiency (IQE) of the MQWs forming the active region must also be taken into account. The IQE is determined by the interplay of the radiative and nonradiative recombination. At moderate carrier densities, the dominating type of the nonradiative recombination is the Shockley-Read-Hall (SRH) recombination through impurities and point defects.⁷⁾ Replacing GaN with InGaN as the barrier material might affect both the radiative and SRH recombination rates. For instance, the concentration of N vacancies and related complexes that act as SRH recombination centers might be increased.8) On the other hand, there have been reports that in QWs with InGaN barriers the SRH recombination rate is lower.⁶⁾

Thus, to determine barrier parameters that are optimal for light emitting devices, the IW carrier transport should be studied along with the radiative and nonradiative lifetimes and, ultimately, the IQE. In this work, by exploring these effects in InGaN/(In)GaN MQW structures with different indium percentage in the barriers, we evaluate the interplay between these effects. In addition, to examine the effect that ternary barriers with a higher band gap might have on the IW transport, MQW structures with AlGaN barriers were explored. A recent study has suggested that AlGaN barriers might be advantageous for near-ultraviolet InGaN LEDs. 9)

The studied structures were grown by metal-organic chemical vapor deposition on *c*-plane sapphire substrates.

From the substrate side, the structures consist of a 4.3 μ m GaN buffer layer, a 3 nm thick InGaN detector QW (DQW) with 16%–18% In, a region of four 3 nm thick transport QWs (TQWs) with ~12% In, and a 100 nm thick GaN cap layer (inset to Fig. 2). For different samples, the In content in the 8 nm thick InGaN barriers is 0%, 4% and 6%. In one sample, the barrier material is Al_{0.065}Ga_{0.935}N. The structures are unintentionally n-doped with an electron concentration of ~1 × 10¹⁷ cm⁻³. The threading dislocation density, estimated by plan view transmission electron microscopy and atomic force microscopy, was 2 × 10⁸ cm⁻² for all samples. The surface topography of the samples was identical; thus, observed differences in the PL intensity were intrinsic and unrelated to different light extraction efficiencies.

The measurements were performed by time-resolved and time-integrated photoluminescence (PL) spectroscopy. The PL was excited by second and third harmonic pulses from a self-mode-locking Ti:sapphire laser with a 200 fs pulse duration and central wavelengths of 260, 390, and 430 nm. The different wavelengths allowed resonant carrier excitation in layers with different band gaps. In particular, the 260 nm excitation generated electron-hole pairs primarily in the cap layer, the 390 nm excitation—in the QWs, and 430 nm—in the DQW. To assure that long PL transients were measured without the carrier build-up, the laser pulse repetition rate of 80 MHz was reduced to 4 MHz with an acousto-optic pulse picker. PL transients were registered with a time-correlated single photon counter (temporal response 50 ps) after selecting regions of the TQW and DQW emission with band pass filters. Time-integrated PL spectra were recorded using a spectrometer with a liquid nitrogen-cooled charge-coupled device detector array. The measurements were performed in the temperature range from 12 to 340 K.

Time-integrated PL spectra of different samples at 300 K, normalized to the TQW PL intensity, are presented in Fig. 1. The DQW PL was dominating the spectra of the InGaN barrier structures. For the GaN and AlGaN barrier structures, the signal from the TQWs was prevalent. The large difference in the DQW/TQW PL intensity ratio shows that the number of carriers that reach the DQW strongly depends on the barrier height.

The IW carrier transport was evaluated from the rising part of DQW PL transients using an optical marker technique. 5,10-12) For the 260 nm excitation, most of the

¹Department of Applied Physics, KTH Royal Institute of Technology, AlbaNova University Center, 10691 Stockholm, Sweden

²Materials Department, University of California, Santa Barbara, California 93106, United States of America

^{*}E-mail: yapparov@kth.se

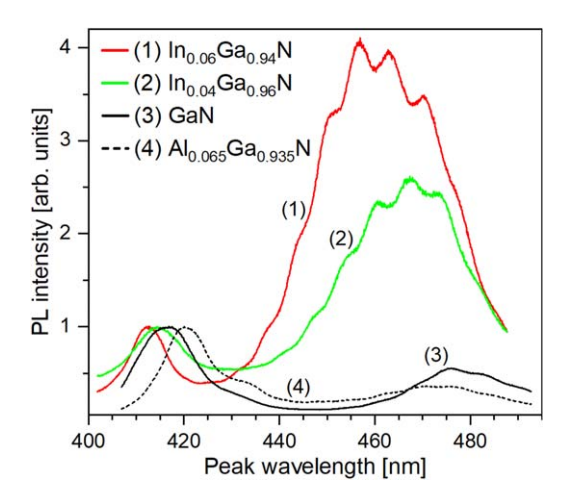


Fig. 1. (Color online) PL spectra of studied samples at 300 K. Fringe patterns originate from Fabry–Perot interference.

electron-hole pairs are generated in the cap layer. In a few tens of ps after the excitation, these carriers are captured into the first TQW.⁵⁾ After passing the TQWs, the photoexcited carriers end up in the DQW; hence, the rise of the DQW PL signal reflects the process of the carrier transfer through the TQW region. For the IW transport measurements, the excitation pulse energy was 25 pJ corresponding to the initial photoexcited carrier density in the GaN layer of about $5 \times 10^{17} \, \text{cm}^{-3}$. In the TQWs, the initial carrier concentration was of the order of $1 \times 10^{19} \text{ cm}^{-3}$. The latter value was estimated taking into account that PL decay time, measured at the GaN band gap energy (45 ps, determined with a streak camera), was much shorter than GaN radiative and nonradiative recombination times of about 5 ns and 0.5 ns, respectively, 13,14) and that the carrier capture to the first TQW is much more efficient than trapping to the surface states.⁵⁾ Since the photoexcited carrier density was considerably larger than the unintentional n-doping, the IW transport was ambipolar and governed by the slower holes.⁵⁾

300 K PL transients for the DQWs of the different structures are presented in Fig. 2. One can notice that the transients contain fast (instantaneous on the scale of Fig. 2) and slow components of the PL increase. These components reflect radiative recombination of carriers generated in

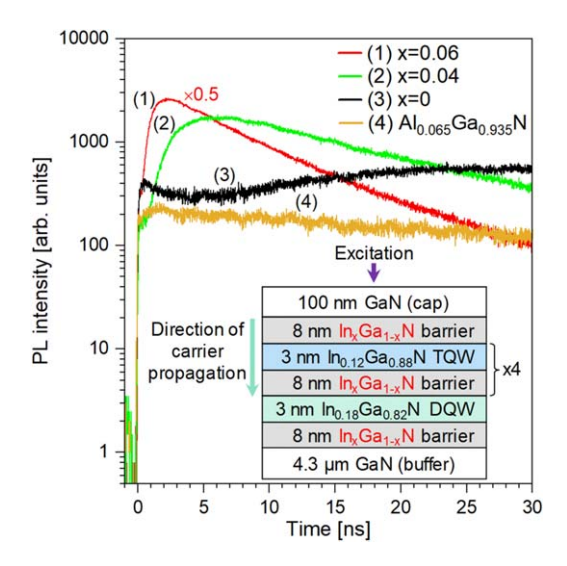


Fig. 2. (Color online) 300 K DQW PL transients for the studied structures.

different regions of the structures. The fast component arises from the recombination of carriers excited directly in the DQW and adjacent barriers. The slow component accounts for carriers excited in the cap layer and transferred to the DQW via the TQWs.

For the AlGaN barrier structure, the slow PL rise component is absent indicating that carriers excited in the GaN cap layer do not reach the DQW. Thus, the advantage of using AlGaN barriers for violet InGaN QW LEDs reported in Ref. 9 must be related to effects other than the uniform IW carrier distribution and reduced Auger recombination.

For the structure with GaN barriers, the slow PL rise component extends for a few tens of ns (its initial part in the interval 0–5 ns is masked by the decay of carriers excited directly into the DQW). This shows that the carrier transport via the TQW region is slow. Moreover, the contributions to the DQW PL signal at ~ 30 ns from carriers excited in the cap layer and directly into the DQW are comparable, even though the numbers of carriers generated in the respective regions differ by a factor of ~ 50 . This explicitly shows that in the GaN barrier structure the IW hole transport is inefficient.

On the other hand, for the InGaN barrier structures the slow PL rise is much shorter, extending during 0–4 ns for the structures with 4% In and 0–2 ns for the 6% In barriers, respectively. This demonstrates that the IW carrier transfer in the InGaN barrier structures is fast and efficient. In the further discussion we will concentrate on these structures using the GaN barrier structure as a reference.

The PL rise times were evaluated by fitting PL transients with an empirical equation

$$I_{\rm PL}(t) = A \left(\exp\left(-\frac{t}{\tau_r}\right) - \exp\left(-\frac{t}{\tau_d}\right) \right),$$
 (1)

where τ_r and τ_d are the (slow) rise and decay times respectively, and A is a proportionality constant. The IW transport time per TQW was calculated by dividing the slow DQW PL rise time by the number of TQWs, i.e. 4. These transport times for the structures with GaN, 4% and 6% In barriers at 300 K are listed in Table I.

DQW PL transients at different temperatures for the InGaN barrier structures are shown in Fig. 3. As the temperature is increased, the PL rise times become shorter, in agreement with the previous measurements on similar structures. Analysis of the temperature dependence of the PL rise times indicates that the mechanism limiting the IW transport is the thermionic transport of holes. The thermionic emission time τ_{TE} depends on the effective barrier height ΔE exponentially, $\tau_{\text{TE}} \propto \exp(\Delta E/kT)$; hence, the large difference in between the transport times for the different structures is a direct consequence of the different barrier heights. Activation energies, extracted from the PL rise time dependence on the

Table I. Transport and recombination times for the MQW structures with different barriers.

Type of barriers	GaN	In _{0.04} Ga _{0.96} N	In _{0.06} Ga _{0.94} N
IW transport time, ns	2.5	0.5	0.2
TQW, radiative lifetime, ns	12	12	3.3
TQW, nonradiative lifetime, ns	14	3.9	1.3
TQW relative IQE, %	59	27	29
DQW, nonradiative lifetime, ns	67	7.1	2.9

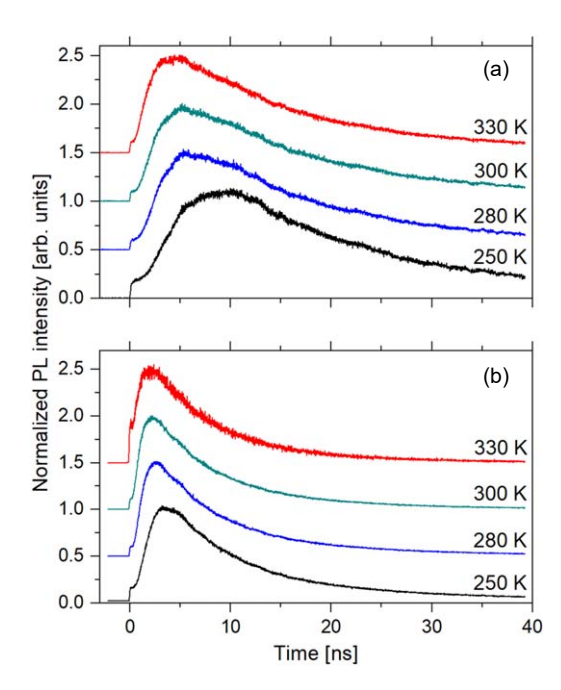


Fig. 3. (Color online) Normalized transients of the DQW PL at different temperatures for the structures with 4% (a) and 6% (b) of indium in the barriers.

inverse temperature, are 110 meV and 90 meV for the 4% and 6% In barrier structures, respectively. This can be compared to the hole confinement energies of 80 meV and 50 meV, respectively, obtained from a solution of Schrödinger equation for a valence band offset of 0.3. The activation energies exceeding the confinement energies show that the IW transport is also affected by the band potential tilt in the barriers.⁵⁾

As mentioned in the introduction, the fast IW transport and uniform carrier distribution in the MQWs is not the only effect determining efficiency of the high power LEDs. The IW transport should be analyzed along with the IQE, which might be affected by replacing GaN barriers with that of InGaN.

The IQE η was evaluated from the radiative and nonradiative recombination times according $\eta = \tau_{\rm NR}/(\tau_R + \tau_{\rm NR})$, where $\tau_{\rm NR}$ and τ_R are the nonradiative (SRH) and radiative recombination times, respectively. The nonradiative recombination time was calculated from the PL decay time τ_{PL} and the radiative lifetime following $1/\tau_{\rm NR} = 1/\tau_{\rm PL} - 1/\tau_{\it R}$. The PL decay time was extracted from single-exponential fits of the PL decay. The radiative lifetime at different temperatures was evaluated from PL transient amplitudes taking into account that the radiative lifetime is inversely proportional to this amplitude. 16-18) It was also assumed that at 12 K and at early times after the excitation the recombination is purely radiative. The latter assumption is not entirely strict since some SRH recombination might take place even at low temperatures via carrier tunneling into deep recombination centers. 19) Hence, the estimated IQE is the upper limit of the real IQE and will be referred to as relative IQE. One should note that the used approach for the IQE evaluation is more accurate than the one based on comparison of time-integrated PL intensities since it has weaker requirements for the low temperature IQE (100%) at early times after excitation rather than at all times) and allows avoiding the impact of the measurement transfer function variation.

The PL decay, radiative and nonradiative recombination times for the TQWs of the InGaN barrier structures are presented in Fig. 4. For estimation of the recombination times, it is important that no carrier transport between the cap layer and TQWs, and between the TQWs and DQW would take place. This was achieved by using excitation below the GaN band gap at 390 nm. Because of the small thickness of the absorbing material (five 3 nm thick QWs), the photoexcited carrier density was low, and there was no carrier distribution between the TQWs and DQW. This was confirmed by the absence of the slow rise component for the DQW PL, which would have signaled the carrier transfer from the transport wells. Consequently, the TQW PL decay was determined solely by the recombination in these QWs. The difference for the 260 nm (used to evaluate the IW transport) and 390 nm excitation is that in the latter case the photoexcited carrier concentration is much lower allowing for the holes to localize at deep sites from which the thermionic emission over the barriers is not efficient.

From Fig. 4 one can notice several trends. Firstly, the radiative lifetime, which is relatively constant at low temperatures, at about 250 K starts increasing. This effect can be assigned to the change of the prevailing radiative recombination mode from excitonic to free carrier. At about the same temperature the SRH recombination, being weak at low temperatures, becomes the dominant recombination channel.

With increased In content in the barriers, both τ_R and τ_{NR} decrease (Table I). First, let us discuss the barrier composition dependence of the radiative recombination time. The radiative lifetime, which is proportional to the squared electron and hole wave function overlap, is affected by the vertical electric field, which in InGaN QWs is primarily caused by the piezoelectric effect, 22) and by the electron and hole separation in the QW plane, caused by the carrier localization at different sites. ^{23–28)} The vertical wave function overlap can be estimated by self-consistently solving onedimensional (1D) Schrödinger and Poisson equations. To that end, we have used a solver of Ref. 29. The squared overlap integrals are 0.32, 0.41 and 0.47 for the QWs with GaN, In_{0.04}Ga_{0.96}N and In_{0.06}Ga_{0.94}N barriers, respectively. These values, although confirming the general trend that the radiative lifetimes decrease with decreasing barrier height, considerably differ from the experimental data (Table I), especially for the structure with 6% indium in the barriers.

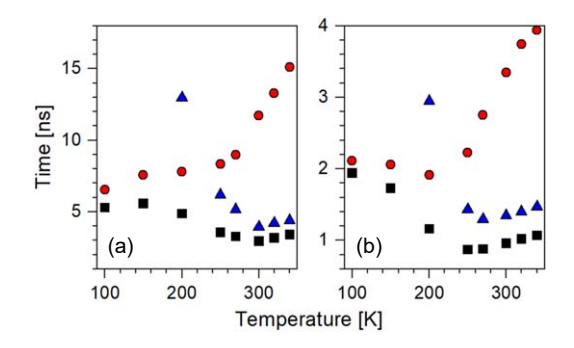


Fig. 4. (Color online) Radiative (circles), nonradiative (triangles) and PL decay times (squares) for the TQWs of (a) $In_{0.04}Ga_{0.96}N$ and (b) $In_{0.06}Ga_{0.94}N$ barrier samples at different temperatures measured with 390 nm excitation.

This deviation shows that the 1D band structure models are too simplified since they do not take into account the in-plane wave function separation. This effect is more important for QWs with higher barriers for which either both electrons and holes or only holes are localized. 26,30) The large decrease of the radiative lifetimes for the 6% In barrier QWs compared to those with GaN and In_{0.04}Ga_{0.96}N barriers is most probably related to the carrier delocalization in the 6% In barrier case. The calculated confinement potentials for these QWs are by a factor of 0.6 smaller than for the wells with 4% In barriers (50 and 80 meV for the valence band). Since the range of the band potential fluctuations is proportional to the confinement energy,³⁰⁾ it is likely that for the 6% In barriers the effect of the lateral electron and hole function separation is much smaller due to the electron, and possibly even hole delocalization. This would leave only the vertical electron and hole function separation as a factor affecting the radiative lifetime for these OWs.

Decrease of τ_{NR} occurs due to an increased SRH recombination. The latter effect may take place in the TQWs, InGaN barriers, or at the QW/barrier interfaces. The relevance of these recombination channels can be assessed by comparing the recombination times in the transport and DQWs of the different structures.

The DQWs are much deeper than the TQWs; the probability for holes to be thermally excited into the barriers from the DQWs is about 60 times smaller than from the TQWs. For electrons this ratio is even larger, of the order of 2×10^3 . However, the experimental values of the nonradiative lifetimes do not experience such a large difference. For the 6% In barrier structure, τ_{NR} for the TQWs and DQW are similar; for the 4% In barriers, the nonradiative recombination time of the DQW is longer by just a factor of 2. In addition, the InGaN barriers were grown under identical conditions except for the trimethylindium flow; thus, the concentration of the SRH recombination centers should have little dependence on the In content. Consequently, the nonradiative recombination in the barriers is not the primary cause of the increased nonradiative recombination in the InGaN barrier structures.

The relevance of the nonradiative recombination in the QWs can be evaluated by comparing the PL decay times in the GaN and InGaN barrier structures. All the structures were grown in subsequent runs, and the QW layers were deposited under identical conditions. Hence, the SRH center concentrations in the QWs are expected to be similar, independently whether the barriers are composed of GaN or InGaN. However, the recombination times for the GaN barrier structure are much longer (Table I). This means that the QWs themselves are not the main channels of the SRH recombination. Consequently, the increased nonradiative recombination in the InGaN barrier structures should be assigned to the third possible channel of the SRH recombination, namely, the InGaN/InGaN QW interfaces.

The impact of the nonradiative recombination at the interfaces could probably be reduced by the barrier engineering, e.g. by surrounding the InGaN barriers with thin GaN layers. Insertion of 1.3-monolayer thick low temperature grown GaN interlayers has been reported to improve the InGaN MQW LED performance.³¹⁾ The improvement has been assigned to a decreased intermixing between the well

and barrier layers and smoother interfaces leading to a reduced SRH recombination.

However, even the simple InGaN barriers used in this study might be advantageous over the GaN barriers for MQW devices operating in the high current regime. This supposition is related to the different power dependence on the carrier density for Auger (cubic) and SRH (linear) nonradiative recombination rates and may be demonstrated by a simple numerical estimation.

Let us consider two borderline cases for LED structures with the 4 QWs in the active region and the same number of injected carriers. In the first one, the carriers would distribute evenly between the QWs (the low barrier case). In the second one, because of the high barriers and inefficient IW hole transport, all carriers would accumulate in the QW closest to the *p*-side of the structure. 1) Further on, let us assume that the carrier concentration in the QWs of the low barrier structure is $7.5 \times 10^{18} \, \text{cm}^{-3}$, a typical value for an LED operating at a high current. For the high barrier structure, the carrier density in the active QW would be $3 \times 10^{19} \, \text{cm}^{-3}$. For such carrier density and a typical Auger coefficient 3×10^{-31} cm⁶ s⁻¹, ³²) the Auger recombination time would be about 4 ns. This is close to the SRH recombination time for the 4% InGaN barrier structure measured at moderate carrier densities. Moreover, since the SRH centers are seldom ideal recombination centers with equal electron and hole capture rates, the SRH recombination at high carrier densities tends to saturate increasing the recombination time.⁷⁾ This would make the relative weight of the Auger recombination even more pronounced. For the uniform carrier distribution between the 4 wells, the rate of the Auger recombination would be 16 times lower making the overall rate of the nonradiative recombination smaller compared to the case of the carrier accumulation in one QW.

Comparing the structures with 4% and 6% indium in the barriers one should note that both have low IW transport times that are considerably shorter than the recombination times, and similar relative IQEs. The structure with the 6% In barriers should be distinguished as having a much shorter IW transport time and short radiative lifetime, which increases the IQE. One should note, however, that 6% In for the barriers of $In_{0.12}Ga_{0.88}N$ QWs is probably the limit because lowering the barriers even further would cause a loss of the carrier confinement in the QWs.

In summary, the influence of barrier composition on the interwell carrier transport in In_{0.12}Ga_{0.88}N/(In)GaN MQWs was studied by the time-resolved PL using the optical marker technique. The study was complemented by measurements of the relative IQE. With introduction of In into the barriers, the IW transport time was reduced by a factor of 5 for the In_{0.04}Ga_{0.96}N barrier structure and by a factor of 12 for the structure with In_{0.06}Ga_{0.94}N barriers. The relative IQE, however, in the InGaN barrier structures was about two times lower compared to the structure with GaN barriers. It is suggested that the main nonradiative recombination channel is the carrier recombination at the QW interfaces, which might be reduced by inserting thin GaN layers at the QW and barrier boundaries. Even without such reduction, advantage of the uniform carrier distribution and reduced Auger recombination for light emitting devices operating in the high current regime might overcome the drawback of the somewhat lower IQE suggesting a viable path in the development of high power GaN-based light emitters.

Acknowledgments Research at KTH was financially supported by the Swedish Energy Agency (Contract No. 45390-1). Research at UCSB was supported by the U.S. Department of Energy under Award No. DE-EE0008204. Additional support for the work at UCSB (JSS) came from the Simons Foundation through Award No. 601952 and the NSF RAISE-TAQS program (NSF award # 1839077 through a subcontract to the University of Minnesota subaward A007231601).

ORCID iDs Rinat Yapparov https://orcid.org/0000-0001-8496-9668

- A. David, M. J. Grundmann, J. F. Kaeding, N. F. Gardner, T. G. Mihopoulos, and M. R. Krames, Appl. Phys. Lett. 92, 053502 (2008).
- 2) Y.-K. Kuo, T.-H. Wang, and J.-Y. Chang, Appl. Phys. Lett. **100**, 031112 (2012).
- 3) W. G. Scheibenzuber and U. T. Schwarz, Appl. Phys. Express 5, 042103 (2012).
- D. S. Sizov, R. Bhat, A. Zakharian, K. Song, D. E. Allen, S. Coleman, and C. Zah, IEEE J. Sel. Top. Quantum Electron. 17, 1390 (2011).
- S. Marcinkevičius, R. Yapparov, L. Y. Kuritzky, Y.-R. Wu, S. Nakamura, S. P. DenBaars, and J. S. Speck, Appl. Phys. Lett. 114, 151103 (2019).
- M. Ikeda, F. Zhang, R. Zhou, J. Liu, S. Zhang, A. Tian, P. Wen, L. Zhang, D. Li, and H. Yang, Jpn. J. Appl. Phys. 58, SCCB03 (2019).
- A. Rashidi, M. Monavarian, A. Aragon, and D. Feezell, Sci. Rep. 9, 19921 (2019).
- A. Haller, J.-F. Carlin, G. Jacopin, W. Liu, D. Martin, R. Butté, and N. Grandjean, Appl. Phys. Lett. 113, 111106 (2018).
- Y. Li, Z. Xing, Y. Zheng, X. Tang, W. Xie, X. Chen, W. Wang, and G. Li, J. Mater. Chem. C 8, 883 (2020).
- B. Deveaud, J. Shah, T. C. Damen, B. Lambert, and A. Regreny, Phys. Rev. Lett. 58, 2582 (1987).
- 11) K. Fröjdh, S. Marcinkevičius, U. Olin, C. Silfvenius, B. Stålnacke, and G. Landgren, Appl. Phys. Lett. 69, 3659 (1996).
- 12) H. Hillmer and S. Marcinkevičius, Appl. Phys. B 66, 1 (1998).
- 13) O. Brandt, J. Ringling, K. H. Ploog, H.-J. Wünsche, and F. Henneberger, Phys. Rev. B 58, R15977 (1998).

- 14) T. K. Uždavinys, S. Marcinkevičius, J. H. Leach, K. R. Evans, and D. C. Look, J. Appl. Phys. 119, 215706 (2016).
- 15) H. Schneider and K. von Klitzing, Phys. Rev. B 38, 6160 (1988).
- 16) E. Berkowicz, D. Gershoni, G. Bahir, E. Lakin, D. Shilo, E. Zolotoyabko, A. C. Abare, S. P. DenBaars, and L. A. Coldren, Phys. Rev. B 61, 10994 (2000).
- S. Marcinkevičius, K. M. Kelchner, L. Y. Kuritzky, S. Nakamura, S.
 P. DenBaars, and J. S. Speck, Appl. Phys. Lett. 103, 111107 (2013).
- 18) T. Langer, M. Klisch, F. A. Ketzer, H. Jönen, H. Bremers, U. Rossow, T. Meisch, F. Scholz, and A. Hangleiter, Phys. Status Solidi B 253, 133 (2016).
- 19) R. Pässler, Phys. Status Solidi B 85, 203 (1978).
- M. Gurioli, J. Martinez-Pastor, M. Colocci, C. Deparis, B. Chastaingt, and J. Massies, Phys. Rev. B 46, 6922 (1992).
- 21) L. C. Andreani, Solid State Commun. 77, 641 (1991).
- 22) F. Bernardini and V. Fiorentini, Appl. Surf. Sci. 166, 23 (2000).
- 23) D. Watson-Parris, M. J. Godfrey, P. Dawson, R. A. Oliver, M. J. Galtrey, M. J. Kappers, and C. J. Humphreys, Phys. Rev. B 83, 115321 (2011).
- 24) R. Ivanov, S. Marcinkevičius, Y. Zhao, D. L. Becerra, S. Nakamura, S. P. DenBaars, and J. S. Speck, Appl. Phys. Lett. 107, 211109 (2015).
- 25) D. S. P. Tanner, M. A. Caro, E. P. O'Reilly, and S. Schulz, RSC Adv. 6, 64513 (2016).
- 26) R. Ivanov, S. Marcinkevičius, M. D. Mensi, O. Martinez, L. Y. Kuritzky, D. J. Myers, S. Nakamura, and J. S. Speck, Phys. Rev. Appl. 7, 064033 (2017).
- 27) R. Ivanov, S. Marcinkevičius, T. K. Uždavinys, L. Y. Kuritzky, S. Nakamura, and J. S. Speck, Appl. Phys. Lett. 110, 031109 (2017).
- 28) T. K. Uždavinys, D. L. Becerra, R. Ivanov, S. Nakamura, S. P. DenBaars, J. S. Speck, and S. Marcinkevičius, Opt. Mater. Express 7, 3116 (2017).
- 29) H. Hebal, Z. Koziol, S. B. Lisesivdin, and R. Steed, Comput. Mater. Sci. 186, 110015 (2021).
- C. Mounir, U. T. Schwarz, I. L. Koslow, M. Kneissl, T. Wernicke,
 T. Schimpke, and M. Strassburg, Phys. Rev. B 93, 235314 (2016).
- 31) Y.-K. Kuo, M.-C. Tsai, S.-H. Yen, T.-C. Hsu, and Y.-J. Shen, IEEE J. Sel. Top. Quantum Electron. 15, 1115 (2009).
- 32) E. Kioupakis, Q. Yan, D. Steiauf, and C. G. Van de Walle, New J. Phys. 15, 125006 (2013).